COMMUNICATION

Moisture-Responsive Graphene Paper Prepared by Self-Controlled Photoreduction

Dong-Dong Han, Yong-Lai Zhang, Hao-Bo Jiang, Hong Xia, Jing Feng, Qi-Dai Chen, Huai-Liang Xu, and Hong-Bo Sun**

Smart actuators are devices that can reversibly change their dimensions under certain stimulation or convert various types of energy to mechanical deformation.[1] In recent years, triggered by some distinguished properties, for instance, high sensitivity, fast and reversible response, and intelligence, as well as low energy cost, smart actuators have drawn enormous research interest in many high-tech fields such as robotics,[2] unmanned flight,[3] sensors,[4] in vivo surgery devices[5] and lab-on-a-chip systems.[6,7] To date, a wide variety of novel driving techniques, including electrostatic or piezoelectric actuation,[8] shape-memory alloys,[9] magnetic remote control,[10,11] optical tweezers,[12,13] pneumatic systems,[14] and thermal effects[15] have been successfully adopted for the development of smart actuators. However, for these driving methodologies, external energy-supply systems or coupled instruments are generally necessary, which significantly limits their practical applications.

As an alternative choice, stimuli-responsive materials (SRMs), which show special response to surrounding temperature,[16] pH value,[17] UV light,[18] or solvents,[19] provide the feasibility to design and fabricate smart actuators. However, the response of SRMs is generally isotropic, which significantly limits their complex performance, for instance, bending. To realize desired performance in a predefined fashion, stimuli-responsive structures (SRSs), represented by two-/multilayer structures, have been successfully developed. For instance, Zhang et al. reported the scrolling of multilayered SiGe/Si/Cr nanobelt with width less than 1 μm due to the edge effect.[20] Gracias et al. reported a series of bilayer microgrippers that could be actuated by pH value, temperature, chemicals, and even enzymes.[21–23] Huck et al. give the example of Au-polymer bilayer brush for controlled folding.[24] A general concept for the manipulation of such SRSs is to cause diverse dimension changes in different material layers under certain actuations. In

this case, the strain transition among different material layers is stepwise. Moreover, as a moving component, multilayer SRSs may also suffer from poor interlayer adhesion during frequent bending. Moreover, concerns with respect to toughness, elasticity and chemical/physical stabilities also constitute a main barrier for the development of SRSs-based smart actuators. In this regard, rational design and fabrication of SRSs by refined control of the lateral microstructures of a solo material might be a solution to the above-mentioned problems, but obviously, it is currently challenging.

On the other hand, from the material point of view, graphene and related materials, which exhibit enticing physical/chemical properties such as high electrical conductivity, transparency, biocompatibility, mechanical flexibility, strength, and good stability,[25–29] have revealed great superiority for the development of stimuli-responsive multilayer structures. Consequently, graphene and related materials have been considered as outstanding candidates for smart actuators. Inspired by the bi-/multilayer SRSs reported based on metals, semiconductors, and polymers, for the first time, we present here a preparation of moisture-responsive graphene papers by novel focused sunlight-irradiation-induced photoreduction of graphene oxide (GO). Previous results reported by ours and other groups have already proved that photoreduction of GO is an efficient route for the modulation of the surface/interface properties of GO films through a mask-free, chemical-free, and cost-effective manner.[30–35] In this work, a self-controlled photoreduction of GO paper has been applied to prepare GO/RGO bilayer structures by using sunlight as an irradiation source. Since both sunlight penetration and the subsequent thermal relaxation would be significantly suppressed after forming an expanded RGO layer, photoreduction only occurs on the surface layer of the thick GO paper. In this way, a unique GO/RGO bilayer structure has been successfully prepared in a self-controlled manner. Interestingly, the resultant GO/RGO bilayer paper shows moisture-responsive properties under humid conditions due to anisotropic water-molecule adsorption. Based on the GO/RGO smart paper, novel graphene-based moisture-responsive actuators have been successfully developed.

Figure 1a shows the schematic illustration of the fabrication system for the preparation of GO/RGO bilayer papers. Pristine GO paper was prepared by vacuum filtration of GO aqueous solution, and the as-obtained GO paper was dried in air at room temperature. Interestingly, controllable photoreduction of GO paper was carried out using focused sunlight irradiation. In our experiments, a piece of a quartz coverslip was tightly pressed on the surface of a piece of GO paper to isolate it from

D.-D. Han, Dr. Y.-L. Zhang, H.-B. Jiang, Prof. H. Xia, Prof. J. Feng, Prof. Q.-D. Chen, Prof. H.-L. Xu, Prof. H.-B. Sun
State Key Laboratory on Integrated Optoelectronics
College of Electronic Science and Engineering
Jilin University
2699 Qianjin Street, Changchun 130012, China
E-mail: yonglaizhang@jlu.edu.cn; hbsun@jlu.edu.cn
Prof. H.-B. Sun
College of Physics
Jilin University
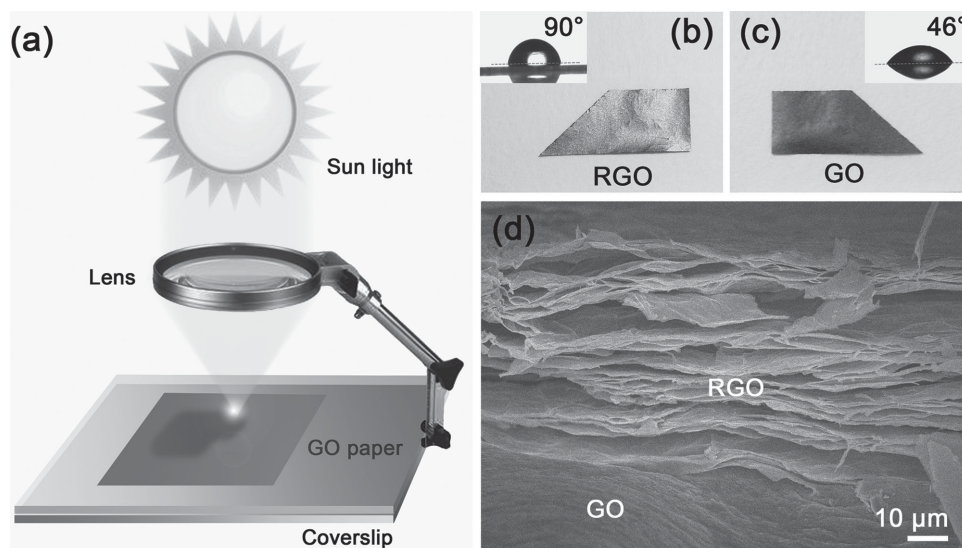119 Jiefang Road, Changchun 130023, China

Figure 1. a) Schematic illustration for the fabrication of GO/RGO bilayer papers using focused sunlight reduction. b,c) Photographs of the resultant GO/RGO bilayer paper viewed from the front side (b) and the reverse side (c), respectively. The insets show water droplet contact angles of both sides. d) SEM image of the section view of GO/RGO bilayer paper.

ambient oxygen. Then incident solar radiation was focused on the surface of the GO paper using a 60 mm-diameter convex lens (focal length = 15 cm, focused spot diameter is ca. 1 mm). To guide the scanning path of the focal spot in a controlled manner, a 2D movable platform with a movement rate of 0.2 mm/s was adopted for the experiments. In our work, a GO paper of 1 cm^2 could be treated within 18 min. Providing a parallel lens array is used for the photoreduction, a much higher efficiency can be achieved, making this sunlight reduction method very promising for the batch production of smart graphene papers. In fact, photoreduction of GO paper occurred as soon as the sunlight was focused on the GO paper, which could be proved by the rapid color change from yellow–brown to black. Since the as-prepared GO solution shows strong absorption in UV region (Figure S1, Supporting Information), the UV light in solar radiation may be essential for GO reduction. To confirm this hypothesis, a sub-400 nm cut-off filter was adopted in the reduction system; in this case, no obvious color change of the GO paper could be observed, indicating the ineffectual reduction of GO paper. This result confirms that the UV light in solar radiation plays a critical role for GO photoreduction.

After the focused sunlight treatments, the color of the resultant GO paper presents a black color with a metallic luster, indicating the thorough reduction of GO (Figure 1b). However, when we observed the reverse side of the RGO paper, it still remained dark brown in color, which reveals the difference in reduction degree (Figure 1c). Static water-droplet contact angle (CA) measurements were applied to characterize the surface wettability of the two sides. As observed in the insets of Figure 1b and c, the front side of the RGO paper shows a significantly increased CA of ca. 90°, whereas the reverse side gives a CA value of ca. 46°, which is similar to that of pristine GO (ca. 45°). Generally, the obvious change in surface wettability could be mainly attributed to the drastic removal of hydrophilic oxygen-containing groups (OCGs), such as hydroxyl, epoxy, and carboxyl groups, during photoreduction.[32,36] Thus, the

obvious difference in surface wettability indicates the different reduction degree of the two sides. A section-view SEM image of the RGO paper also confirmed this result (see Figure 1d). Expanded structures with large gaps between adjacent sheets could be observed in the upside section. Such a feature is very common in some laser-reduced GO films,[37] and the formation of expanded structures is generally attributed to photoreduction-induced emission of carbon species (e.g., CO_2, CO, H_2O, CH_4). However, in the bottom of the section, it remained as a stacked layered structure that was quite similar to pristine GO, which indicates that the focused sunlight reduction shows a certain dependence on GO thickness. In this regard, controllable photoreduction of GO paper could be realized by using simple focused sunlight irradiation.

To get further insight into the formation of such asymmetric section structures, we measured the transmittance spectra of pristine GO paper with different thickness. As shown in Figure S2 in the Supporting Information, with the increase of film thickness, transmittance decreases significantly. Especially, when the thickness reaches 18 µm, transmittance between 200 and 500 nm becomes neglective. As mentioned previously, sub-400 nm UV light plays a critical role for GO reduction. In the case of thick GO paper (in this work, ca. 40 µm), the upper layer of the RGO sheets would prevent the penetration of sub-400 nm UV light; meanwhile, the as-generated expanded structures would effectively suppress thermal relaxation. As a result, an asymmetric GO/RGO bilayer structure formed due to the inefficient photoreduction of the GO, and a self-controlled photoreduction of GO has been proposed for the first time.

Figure 2 shows the characterization of the RGO paper (front side of the GO/RGO paper) and the comparison with pristine GO paper. As shown in Figure 2a, X-ray diffraction (XRD) analysis of pristine GO paper exhibited a layered nanostructure, as evidenced by the diffraction peak at $2\theta = 11.8°$, which corresponds to a d-spacing of 0.75 nm. However, after sunlight photoreduction, the peak of the RGO showed a dramatic shift
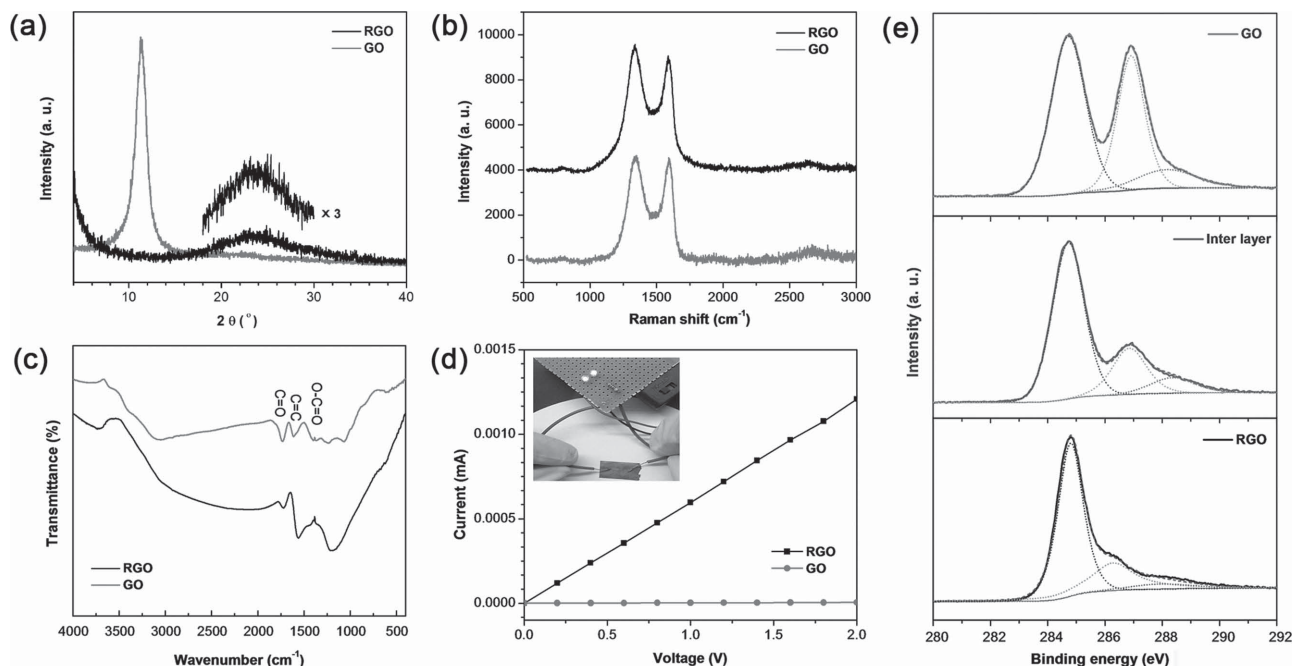
COMMUNICATION

Figure 2. a) XRD patterns of pristine GO paper and the RGO side of the GO/RGO bilayer paper. b) Raman spectra of GO and the RGO paper. c) FTIR spectra of GO and RGO paper. d) Current–voltage (I–V) characteristics of the GO and RGO papers (2 mm × 5 mm), the inset is a photograph of lighting a bubble. e) C1s X-ray photoelectron spectroscopy (XPS) of the reverse side (GO), the interlayer and the front side (RGO) of the GO/RGO bilayer paper.

to much higher 2θ angles (ca. 24°), indicating the significant decrease in interlayer spacing of the RGO sheets (d-spacing ≈ 0.37 nm) after the removal of OCGs. Meanwhile, an obvious broadening of the diffraction peak could be observed, which could be attributed to the smaller sheet size and the irregular stacking of RGO sheets.[38]

It is well known that Raman spectroscopy has been widely used for the characterization of carbon materials. Clearly, the two distinct peaks observed at 1329 and 1589 cm^{-1} correspond to the D and G bands, respectively (Figure 2b). The G band is characteristic of graphite-like structures, whereas the D band is associated with the breathing modes of the graphitic domains, and appears in the presence of defects. Generally, the removal of OCGs would lead to the partially recovery of sp^2 domains, represented by an obvious decrease of D/G intensity ratio (I_D/I_G). However, in our work, the I_D/I_G ratio of RGO sample is somewhat larger than that of pristine GO, which could be explained by the slightly increased defects due to the fragmentation of GO sheets after photoreduction. In our experiment, Fourier transform infrared (FTIR) spectra (Figure 2c) have been adopted to measure the deoxygenation of GO. Notably, pristine GO sample shows a rich collection of transmission bands corresponding to OCGs (e.g., C=O at 1724 cm^{-1}, O–C=O around 1388 cm^{-1}). However, after photoreduction, most of them have been eliminated, which suggests the effective removal of OCGs.

Despite the fact that the graphitic structure could not be recovered after photoreduction, the removal of OCGs would render electrical conductivity to the RGO layer. Generally, the pristine GO paper (2 mm × 5 mm) was electrically insulating, the resistance was measured to be ca. 4.1×10^8 Ω, whereas after photoreduction, its resistance decreased drastically. As shown in Figure 2d, the RGO paper (2 mm × 5 mm) gave an improved

conductivity, and the resistance decreased to 1.66×10^6 Ω. Interestingly, the RGO paper could be used to connect a circuit and light up a bulb, indicating its conductive nature (inset of Figure 2d).

Since the resultant GO/RGO bilayer paper is anisotropic along its lateral section, we used X-ray photoelectron spectroscopy (XPS) to evaluate the reduction degree of the front side, interlayer and reverse side of the GO/RGO paper. Figure 2e shows the C1s XPS of three samples. Notably, the peaks at 284.7, 286.8, and 288.1 eV are attributed to C–C (non-oxygenated ring carbon), C–O (hydroxyl and epoxy carbon) and C=O (carbonyl), respectively. For the reverse side (GO side) of the GO/RGO bilayer paper, the carbon/oxygen mass ratio (C/O) is ca. 2.1, which is almost the same as that of pristine GO. However, when we measured the front side (RGO side) of the GO/RGO bilayer paper, the C/O mass ratio increased to ca. 5.8, indicating the removal of OCGs. The interlayer of the GO/RGO paper was also prepared by a micromechanical cleavage method, similar to the Scotch tape technique. The C/O mass ratio was measured to be ca. 2.7, which is between the GO and RGO sides. These results confirm the unique anisotropy in reduction degree along the lateral section of the GO/RGO bilayer paper.

Interestingly, the GO/RGO bilayer paper shows obvious moisture-responsive bending properties due to this unique lateral anisotropy. To quantitatively investigate their actuating performance, the curvature degrees of a GO/RGO ribbon (width 1.0 mm and length 12 mm) in different relative humidity (RH) were measured, as shown in **Figure 3**. With the increase of RH from 24% to 86%, the curvature of the GO/RGO ribbon increased from gradually 0° to 168°. The insets of Figure 3a show photographs of the bending GO/RGO ribbon under
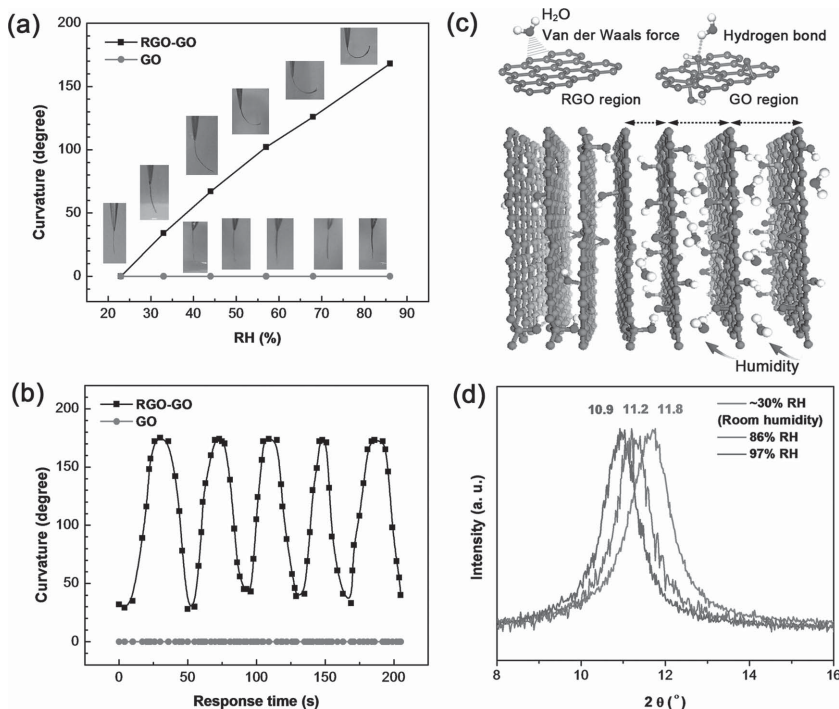
Figure 3. Moisture-responsive properties and mechanism of the GO/RGO bilayer paper. a) Dependence of the curvature of the GO/RGO bilayer paper and pristine GO paper on RH. b) Responsive and recovery properties of the GO/RGO bilayer paper. RH was switched between 33% and 86% five times. c) Schematic illustration of the interaction between water molecules and graphene/GO nanosheets. d) XRD patterns of GO paper under different RHs.

water molecules due to the formation of hydrogen bonds, whereas, in the case of graphene, adsorption of water molecules occurs due to the much weaker Van der Waals forces. In this regard, water molecules would be adsorbed by GO layers in preference to RGO layers, as shown in Figure 3c. The selective adsorption/desorption of water in the GO layers would cause a significant expansion/contraction effect, leading to a reversible bending and straightening performance in moisture and dry conditions, respectively.[39,40] To confirm the mechanism of this moisture-responsive property, we also measured the interlayer spacing of GO sheets under different humidities by XRD (Figure 3d). It is well known that GO paper exhibits a unique layered nanostructure due to the stacking of the GO sheets. Under room humidity (ca. 30% RH), GO paper shows a diffraction peak at ca. 11.8°, which corresponds to an interlayer spacing of ca. 0.75 nm. However, when we increased the humidity to 86% and 97% RH, the diffraction peak moved to 11.2° and 10.9°, respectively, indicating the increase of the interlayer spacing. Notably, under 97% RH, the interlayer spacing of the GO paper was established to be 0.81 nm. These results confirm the mechanism for the bending performance of our GO/RGO bilayer paper under moisture conditions.

different RHs. For comparison, pristine GO paper was also cut into ribbons with the same feature size; however, it could be clearly observed that it do not show any bending performance under different RH. Figure 3b shows the response and recovery characteristics of the GO/RGO bilayer ribbon. When the RH was increased from 33% to 86% RH, the bending curvature increased immediately. It only takes about 15 s to reach equilibrium. On the contrary, when the moisture is decreased to previous value (33%), the bent GO/RGO ribbon recovers its shape completely. The actuation was repeatable upon several cycles, and the bending curvature under different RH was very stable, as shown in Figure 3b.

In addition to the measurement of the bending/straightening performance, the bending/straightening forces of a given GO/RGO ribbon (12 mm × 1 mm, 40 µm thick) were also quantitatively evaluated. The average bending force was measured to be ca. 2.2 mN; and the straightening force was ca. 1.2 mN. Here, it is worth pointing out that the bending and straightening forces show certain dependence on the thickness, width, and length of the GO/RGO ribbon: a GO/RGO ribbon with a larger width would exhibit larger bending/straightening forces. For instance, a GO/RGO ribbon 1.5 mm in width, 12 mm in length, and 40 µm in thickness, gave a bending force of ca. 3.0 mN and a straightening force of ca. 1.6 mN.

In fact, the moisture-responsive property of this GO/RGO bilayer paper is not surprising. In our previous study, we quantificationally investigated the interaction between water molecules and graphene/GO nanosheets by a first-principles study.[32] Generally, GO sheets bearing plenty of OCGs adsorb

The moisture-responsive property of our GO/RGO bilayer paper makes it possible to design and fabricate graphene-based smart actuators. In our work, the unique GO/RGO bilayer papers were firstly cut into ribbons; and then adopted as graphene SRSs directly. **Figure 4**a shows the schematic illustration of the fabrication of a moisture-responsive smart claw, two GO/RGO ribbons were stuck on the wall of a plastic tube, which was connected to a moisture supply system. In this way, the GO/RGO ribbons could act as "smart fingers" for moisture actuation. The GO/RGO ribbons are so sensitive to humidity that they could bend to a certain degree even when approaching a sweaty human finger (Figure 4b). To manipulate the GO/RGO "smart fingers" in a controlled fashion, the plastic tube was connected to a self-made humid- or dry-air supply system, in this manner, the "smart fingers" could be manipulated by changing the humidity, as shown in Figure 4c–e. To further demonstrate their performance, the "smart fingers" were successfully used to pick up a 3 mm cubic polymer foam (Figure 4f–h).

In addition to the "smart fingers" of a moisture-controlled claw, the moisture-responsive GO/RGO bilayer paper could also be used in other smart actuators. **Figure 5** shows two additional examples: an orientable transporter and a crawler paper robot. The former example was prepared by assembling seven GO/RGO ribbons into a linear array. As shown in Figure 5a, by switching the environmental humidity from dry air to moisture, the upright GO/RGO ribbon array would bend in one direction. In this way, the object, the paper slice marked in blue, would be gradually transported to right direction (see Video S1 in the
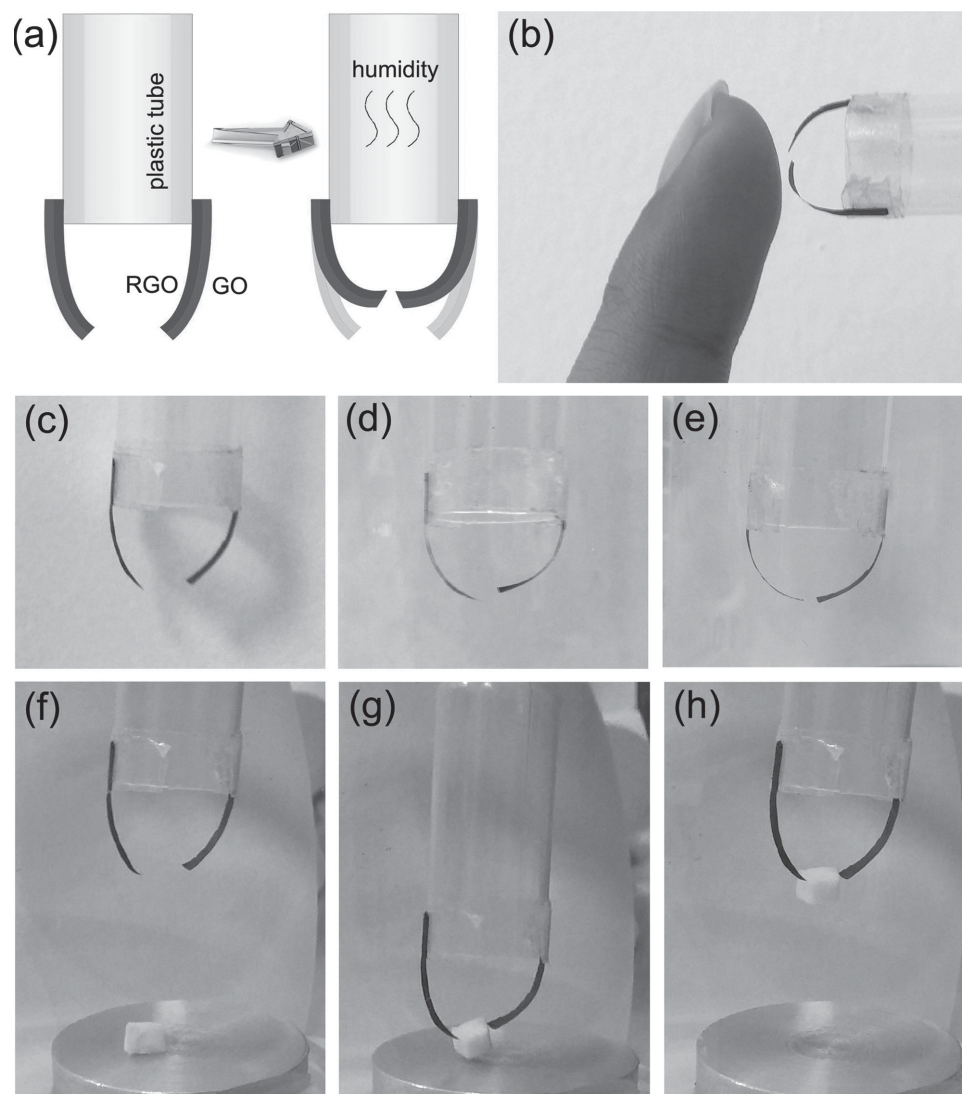
Figure 4. The moisture-responsive performance of a smart claw. a) Schematic illustration of the structure of the smart claw. b) The smart claw is very sensitive to moisture: it could bend when approaching a sweaty human finger. c–e) The moisture responsive claw can be manipulated by controlling the moisture. f–g) The grabbing of a polymer foam block using the smart claw.

Supporting Information). Notably, after 6 cycles of bending and straightening, the paper slice was moved ca. 5 mm, as indicated by the green arrow. The upright GO/RGO ribbon array is so stable that the orientable transporter could be used many times. To experimentally evaluate the stabilities of our smart actuators, both the bending/straightening curvature (between 33% RH and 86% RH) and the bending/straightening force of the GO/RGO ribbon have been measured for 100 times. Experimental results reveal that our moisture responsive GO/RGO ribbon is very stable during frequent bending and straightening. The curvature and the bending/straightening forces almost keep a consistent value after bending for 100 times, indicating the good stability and long cycle lifetime (see Figure S3 and S4, Supporting Information).

For the latter example, two GO/RGO ribbons were appointed as "smart legs" for a moisture-responsive crawler paper robot. As shown in Figure 5b, two GO/RGO "smart legs" were stuck to a paper-cut with two paper legs, which are marked in red. In this way, a very simple self-supported crawler paper robot was successfully fabricated. Very interestingly, when a moisture environment was applied to the paper robot, the two GO/RGO "smart legs" gathered up, leading to a significant bending performance toward the right; whereas when moisture was replaced by dry air, the "smart legs" became unbent, and this performance pushed the whole paper robot toward the right. In our experiment, by switching the moisture/dry air once, the paper robot could move ca. 2 mm. In fact, the moving speed shows a certain dependence on the length of the GO/RGO "smart legs". These results indicate that the moisture-responsive GO/RGO bilayer paper holds great promise for the development of smart actuators. Furthermore, considering the fact that the manipulation of such actuators could be achieved without any energy-supply systems; and graphene has exhibited a lot of
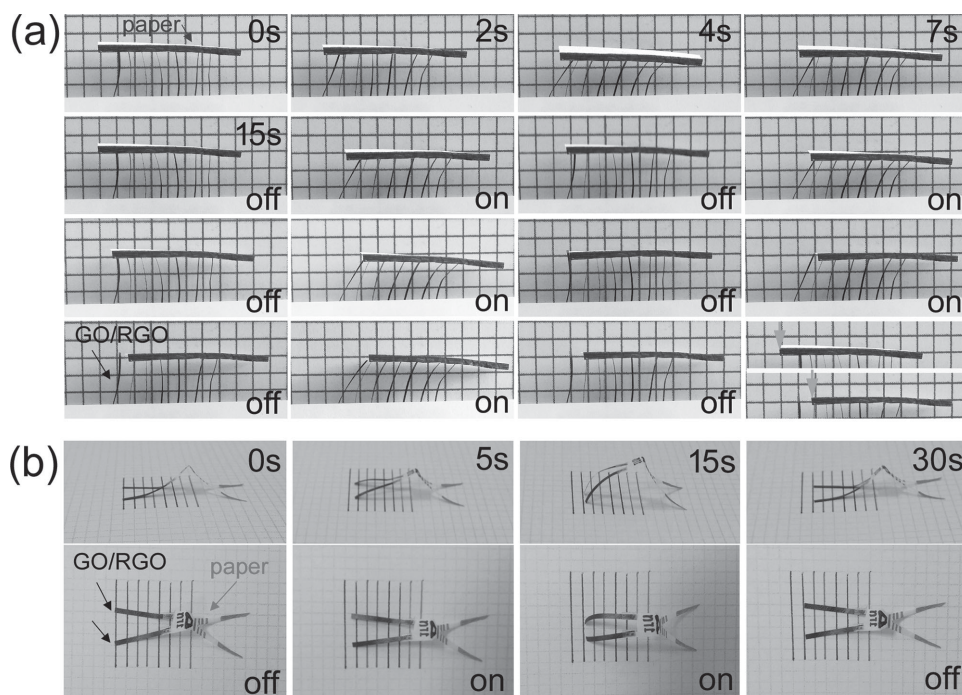
Figure 5. a) An orientable transporter fabricated by assembling 7 upright GO/RGO ribbons into a linear array. The transporter could be used to drive a paper slice toward the right. b) A crawler paper robot fabricated by using GO/RGO bilayer paper as smart legs. "On" and "off" means turning on and turning off the humidity, respectively.

unique chemical/physical properties (e.g., conductivity, flexibility, mechanical strength, and biocompatibility), the moisture-responsive GO/RGO paper may find broad applications in some intelligent devices, for example, sensors,[39,41] micro-electro-mechanical system (MEMS),[42] smart textiles,[43] and even tissue engineering.[44,45]

In conclusion, moisture-responsive graphene paper has been successfully prepared using a very simple focused-sunlight-induced photoreduction method. Experimental results confirm that OCGs on the GO sheets of the GO paper could be drastically removed upon focused sunlight irradiation. However, the photoreduction gradient along the lateral direction of the GO paper is governed by the light absorption and subsequent thermal relaxation, so thick GO paper could not be fully reduced to RGO, because the as-formed expanded RGO structure could effectively prevent the sunlight penetration and suppress thermal relaxation. Instead, unique GO/RGO bilayer structures could be prepared in a self-controlled manner. The anisotropic GO/RGO paper shows very sensitive moisture-responsive properties. The bending curvature of a GO/RGO ribbon changed from 0 to 168° when the RH was tuned from 24% to 86%, because the absorption capabilities of water molecules in the GO and RGO layers are quite different under humid conditions. On the basis of this unique property, typical smart actuators including a claw, an orientable transporter, and a crawler paper robot have been demonstrated. As a simple, cost-effective and self-controlled photoreduction method, focused sunlight irradiation shows unique merits for the batch production of GO/RGO bilayer papers; and the moisture-responsive graphene paper may hold great promise for the development of graphene-based smart robots.

Experimental Section

Preparation of GO Paper: GO was synthesized from natural graphite powder using the Hummer's method. The GO paper was prepared by vacuum filtration of the GO aqueous solution through a membrane filter (0.22 μm in pore size), followed by air drying at room temperature. Finally, the GO paper was peeled off for further use.

Sunlight Photoreduction of GO Paper: The self-standing GO paper was tightly sandwiched between two quartz coverslips. In this way, ambient oxygen could be isolated from the GO paper. Then the incident solar radiation was focused on the surface of the GO paper using a 60 mm diameter convex lens (focal length = 15 cm, focused spot diameter ≈ 1 mm). The experiments were carried out during June and August (weather: sunshine; time: 12:00–13:00 pm) in the city of Chanchun, which is at a longitude of 125° east, and at a latitude of 43° north. The average solar radiation intensity in the range of 280–330 nm was measured to be ca. 900 μW/cm². To guide the scanning path of the focal spot in a controlled manner, a two-dimensional movable platform with a movement rate at 0.2 mm/s was adopted for the GO reduction. The focal spot was about 1 mm in diameter; and the scanning step length (the distance between two neighboring scanning paths) was ca. 0.5 mm.

Characterization: SEM images were obtained using a JEOL JSM-7500 field-emission scanning electron microscope (FE-SEM). The water contact angles (CAs) were measured using a Contact Angle Meter SL200B (Solon Tech. Shanghai). Powder X-ray diffraction (XRD) patterns were collected on a Rigaku D/MAX 2550 diffractometer with Cu Kα radiation ($\lambda = 1.5418$ Å). X-ray photoelectron spectroscopy (XPS) was performed using an ESCALAB 250 spectrometer. IR spectroscopy was recorded using an FTIR Nicolet 5700 spectrometer in the 4000–400 cm⁻¹ frequency range, using powdered samples diluted in KBr pellets. Raman spectroscopy were recorded on a Jobin–Yvon T64000 Raman spectrometer equipped with a liquid-nitrogen-cooled argon ion laser at 514.5 nm (Spectra-Physics Stabilite 2017) as the excitation source; the laser power used was about 10 mW at the samples with an average spot size of 1 μm in diameter. Electrical measurements were carried out using a Keithley 2400 source meter. The controlled humidity

environments were achieved using saturated aqueous solutions of CH_3COOK, $MgCl_2$, K_2CO_3, $NaBr$, $CuCl_2$, KCl, and K_2SO_4 in a closed glass vessel at an ambient temperature of 25 °C, which yielded approximately 23, 33, 44, 57, 68, 86, and 97% relative humidity (RH), respectively.

Supporting Information

Supporting Information is available from the Wiley Online Library or from the author. Absorption spectra of GO aqueous solution and the transmittance of GO paper of different thickness, as well as stability tests of the GO/RGO paper are provided.

Acknowledgements

[1] P. Brochu, Q. B. Pei, *Macromol. Rapid Commun.* **2010**, *31*, 10.

[2] S. Maeda, Y. Hara, R. Yoshida, S. Hashimoto, *Adv. Robotics.* **2008**, *22*, 1329.

[3] S. M. Azizi, K. Khorasani, *Int. J. Control.* **2011**, *84*, 876.

[4] G. Lindner, *J. Phys. D Appl. Phys.* **2008**, *41*, 123002.

[5] L. Zhang, T. Petit, Y. Lu, B. E. Kratochvil, K. E. Peyer, R. Pei, J. Lou, B. J. Nelson, *ACS Nano* **2010**, *4*, 6228.

[6] L. Zhang, K. E. Peyer, B. J. Nelson, *Lab Chip* **2010**, *10*, 2203.

[7] Y. Tian, Y. L. Zhang, J. F. Ku, Y. He, B. B. Xu, Q. D. Chen, H. Xia, H. B. Sun, *Lab Chip* **2010**, *10*, 2902.

[8] S. Sridaran, S. A. Bhave, *Opt. Express* **2011**, *19*, 9020.

[9] A. Villanueva, C. Smith, S. Priya, *Bioinspiration Biomimetics* **2011**, *6*, 036004.

[10] H. Xia, J. A. Wang, Y. Tian, Q. D. Chen, X. B. Du, Y. L. Zhang, Y. He, H. B. Sun, *Adv. Mater.* **2010**, *22*, 3204.

[11] S. Tottori, L. Zhang, F. M. Qiu, K. K. Krawczyk, A. Franco-Obregon, B. J. Nelson, *Adv. Mater.* **2012**, *24*, 811.

[12] S. Kawata, H. B. Sun, T. Tanaka, K. Takada, *Nature.* **2001**, *412*, 697.

[13] M. Gu, H. Bao, X. Gan, N. Stokes, J. Wu, *Light: Sci. Appl.* **2014**, *3*, e126.

[14] R. V. Martinez, A. C. Glavan, C. Keplinger, A. I. Oyetibo, G. M. Whitesides, *Adv. Funct. Mater.* **2014**, *24*, 3003.

[15] V. Percec, M. R. Imam, M. Peterca, P. Leowanawat, *J. Am. Chem. Soc.* **2012**, *134*, 4408.

[16] P. Theato, B. S. Sumerlin, R. K. O'Reilly, T. H. Epps, *Chem. Soc. Rev.* **2013**, *42*, 7055.

[17] Y. L. Sun, W. F. Dong, L. G. Niu, T. Jiang, D. X. Liu, L. Zhang, Y. S. Wang, Q. D. Chen, D. P. Kim, H. B. Sun, *Light: Sci. Appl.* **2014**, *3*, e129.

[18] T. Tatsuma, K. Takada, T. Miyazaki, *Adv. Mater.* **2007**, *19*, 1249.

[19] Y. Tian, Y. L. Zhang, H. Xia, L. Guo, J. F. Ku, Y. He, R. Zhang, B. Z. Xu, Q. D. Chen, H. B. Sun, *Phys. Chem. Chem. Phys.* **2011**, *13*, 4835.

[20] L. Zhang, E. Ruh, D. Grutzmacher, L. X. Dong, D. J. Bell, B. J. Nelson, C. Schonenberger, *Nano Lett.* **2006**, *6*, 1311.

[21] T. G. Leong, A. M. Zarafshar, D. H. Gracias, *Small* **2010**, *6*, 792.

[22] T. G. Leong, C. L. Randall, B. R. Benson, N. Bassik, G. M. Stern, D. H. Gracias, *Proc. Natl. Acad. Sci. USA* **2009**, *106*, 703.

[23] N. Bassik, A. Brafman, A. M. Zarafshar, M. Jamal, D. Luvsanjav, F. M. Selaru, D. H. Gracias, *J. Am. Chem. Soc.* **2010**, *132*, 16314.

[24] T. S. Kelby, M. Wang, W. T. S. Huck, *Adv. Funct. Mater.* **2011**, *21*, 652.

[25] X. S. Li, Y. W. Zhu, W. W. Cai, M. Borysiak, B. Y. Han, D. Chen, R. D. Piner, L. Colombo, R. S. Ruoff, *Nano Lett.* **2009**, *9*, 4359.

[26] Z. S. Wu, W. C. Ren, L. B. Gao, J. P. Zhao, Z. P. Chen, B. L. Liu, D. M. Tang, B. Yu, C. B. Jiang, H. M. Cheng, *ACS Nano.* **2009**, *3*, 411.

[27] C. O. Girit, J. C. Meyer, R. Erni, M. D. Rossell, C. Kisielowski, L. Yang, C. H. Park, M. F. Crommie, M. L. Cohen, S. G. Louie, A. Zettl, *Science* **2009**, *323*, 1705.

[28] M. C. Duch, G. R. S. Budinger, Y. T. Liang, S. Soberanes, D. Urich, S. E. Chiarella, L. A. Campochiaro, A. Gonzalez, N. S. Chandel, M. C. Hersam, G. M. Mutlu, *Nano Lett.* **2011**, *11*, 5201.

[29] N. Papasimakis, S. Thongrattanasiri, N. I. Zheludev, F. G. de Abajo, *Light: Sci. Appl.* **2013**, *2*, e78.

[30] Y. L. Zhang, L. Guo, S. Wei, Y. Y. He, H. Xia, Q. D. Chen, H. B. Sun, F. S. Xiao, *Nano Today* **2010**, *5*, 15.

[31] Y. L. Zhang, Q. D. Chen, H. Xia, H. B. Sun, *Nano Today* **2010**, *5*, 435.

[32] L. Guo, H. B. Jiang, R. Q. Shao, Y. L. Zhang, S. Y. Xie, J. N. Wang, X. B. Li, F. Jiang, Q. D. Chen, T. Zhang, H. B. Sun, *Carbon* **2012**, *50*, 1667.

[33] Y. L. Zhang, L. Guo, H. Xia, Q. D. Chen, J. Feng, H. B. Sun, *Adv. Opt. Mater.* **2014**, *2*, 10.

[34] H. L. Li, C. Bubeck, *Macromol. Res.* **2013**, *21*, 290.

[35] L. J. Cote, R. Cruz-Silva, J. X. Huang, *J. Am. Chem. Soc.* **2009**, *131*, 11027.

[36] J. N. Wang, R. Q. Shao, Y. L. Zhang, L. Guo, H. B. Jiang, D. X. Lu, H. B. Sun, *Chem. Asian J.* **2012**, *7*, 301.

[37] M. F. El-Kady, V. Strong, S. Dubin, R. B. Kaner, *Science* **2012**, *335*, 1326.

[38] W. Gao, L. B. Alemany, L. Ci, P. M. Ajayan, *Nat. Chem.* **2010**, *2*, 1015–1024.

[39] H. H. Cheng, J. Liu, Y. Zhao, C. G. Hu, Z. P. Zhang, N. Chen, L. Jiang, L. T. Qu, *Angew. Chem. Int. Ed.* **2013**, *52*, 10482.

[40] R. R. Nair, H. A. Wu, P. N. Jayaram, I. V. Grigorieva, A. K. Geim, *Science* **2012**, *335*, 442.

[41] Y. Zhao, L. Song, Z. Zhang, L. Qu, *Energy Environ. Sci.* **2013**, *6*, 3520.

[42] C. Martin-Olmos, H. I. Rasool, B. H. Weiller, J. K. Gimzewski, *ACS Nano* **2013**, *7*, 4164.

[43] J. Hu, H. Meng, G. Li, S. I. Ibekwe, *Smart Mater. Struct.* **2012**, *21*, 053001.

[44] S. H. Ku, M. Lee, C. B. Park, *Adv. Healthcare Mater.* **2013**, *2*, 244.

[45] D. Bitounis, H. Ali-Boucetta, B. H. Hong, D. H. Min, K. Kostarelos, *Adv. Mater.* **2013**. *25*, 2258.